SAG: Stars and Galaxies **Vol. 3**, id. 3, 2020 December 28

Detection of intermediate-mass black holes in globular clusters using gravitational lensing

Takayuki TATEKAWA [1,2] and Yuuki OKAMURA [3]
[1]*Department of Social Design Engineering, National Institute of Technology, Kochi College, 200–1 Monobe Otsu, Nankoku, Kochi, 783–8508, Japan*
[2]*Research Institute for Science and Engineering, Waseda University, 3–4–1 Okubo, Shinjuku, Tokyo 169–8555, Japan*
[3]*Department of Electrical Engineering and Information Science, National Institute of Technology, Kochi College, 200–1 Monobe Otsu, Nankoku, Kochi, 783–8508, Japan*
tatekawa@kochi-ct.ac.jp

(Received 2020 October 26; accepted 2020 December 23)

Abstract

Recent observations suggest the presence of supermassive black holes at the centers of many galaxies. The existence of intermediate-mass black holes (IMBHs) in globular clusters has also been predicted. We focus on gravitational lensing as a new way to explore these entities. It is known that the mass distribution of a self-gravitating system such as a globular cluster changes greatly depending on the presence or absence of a central massive object. After considering possible mass distributions for a globular cluster belonging to the Milky Way galaxy, we estimate that the effect on the separation angle of gravitational lensing due to an IMBH would be of milliarcsecond order.

Key words: gravitational lensing — intermediate-mass black holes — globular clusters

1. Introduction

The existence of supermassive black holes (SMBHs) at the centers of galaxies have been made evident by recent observations. For example, the shadow of the SMBH in the center of M 87 was directly observed by the Event Horizon Telescope (EHT: Event Horizon Telescope Collaboration et al. 2019). Long-term observations of the movement of stars surrounding the center of the Milky Way Galaxy suggest the existence of an invisible massive object, Sgr A*, considered to be an SMBH (Ghez et al. 2000; Gillessen et al. 2009). For other galaxies, the existence of SMBHs is indirectly suggested by the M–σ relation between the mass of the SMBH and the velocity dispersion of stars in a galaxy (Silk and Rees 1998; Ferrarese and Merritt 2000; Gebhardt et al. 2000; Gültekin et al. 2009).

The question of how SMBHs form has not yet been definitively answered, although various scenarios have been considered over the years (Rees 1984). One of the scenarios involves an intermediate-mass black hole (IMBH: Greene et al. 2020) that grows to become an SMBH. On the basis of the M–σ relation, it seems possible that IMBHs may be located at the centers of globular clusters. This has been discussed particularly in the case of M 15 but has not been resolved (Gerssen et al. 2002; Baumgardt et al. 2003; McNamara et al. 2003; Kiselev et al. 2008; Murphy et al. 2011; den Brok et al. 2014), although indirect verification has been performed using statistical properties of stars.

In this paper, we consider a new method of detecting SMBHs and IMBHs. These celestial objects' immense mass bends the trajectory of light from background objects: the gravitational lensing (GL) effect. It can cause background objects to be observed multiple times, and single images to be brightened. Through the GL effect, it is possible to verify the existence of a massive object between the background light-source and the Earth.

GL by globular clusters has been discussed in the past. Kains et al. (2016, 2018) proposed a method for IMBH detection using gravitational microlensing. Bukhmastova (2003) has attempted to explain QSO-galaxy associations using the GL effect produced by globular clusters.

GL is a small effect even for SMBHs; our treatment includes lensing by both the massive object and the surrounding stars. The density profile of the stars in the cluster may be obtained from the equilibrium solution for a gravitational many-body system; it varies greatly depending on the presence or absence of a massive central object. In this paper, we assume a spherically symmetric distribution of stars and analyze the GL effect for various characteristic density profiles.

The paper is organized as follows. In section 2, we discuss the mass distribution for globular clusters. Two models of the distribution are described: 1) a model based on the static state of self-gravitating systems and 2) a phenomenological model. If there is an IMBH in a globular cluster, the surrounding stars are thought to form a cusp. Therefore, the two models are also evaluated with such a cusp, so that in all we consider four types of models in this paper. In section 3, the geodesic equation for light trajectories is discussed. Since the models assume spherical symmetry, the spacetime can be described by

the Schwarzschild metric. We consider the gravitational potential of each model in this metric. If the cusp is distributed across the entire area, the mass will diverge. Hence, it is necessary to connect the spacetime inside the cusp smoothly with that of the cuspless model. In section 4, we compare the GL effect in mass distribution models with/without an IMBH, and estimate the maximum separation angle caused by GL. The difference in the separation angle is found to be of sub-milliarcsecond order when we assume that the lensing object is a globular cluster in the Milky Way Galaxy. In section 5, the conclusions of this study are presented.

2. Mass distribution

2.1. Mass distribution for globular clusters

In this subsection, we explain mass distributions for globular clusters. For simplicity, we assume a spherically symmetric distribution and consider the equilibrium solution in a self-gravitating system under Newtonian gravity. Although the distribution function, in general depends on both energy and angular momentum, we assume that the effect of angular momentum is small and only the energy dependence needs be considered. In this case, the velocity dispersion is isotropic at each point in space, and the energy for matter is given by the kinetic and potential energies.

The distribution function tells us both the distribution of the matter in the system and the velocity at which it moves. The stars in the cluster may be thought of as a fluid obeying an equation of continuity, the collisionless Boltzmann equation, that contains a term depending on the gradient of a potential. Suppose that the distribution function is a known function of energy, and that the potential in the collisionless Boltzmann equation is the gravitational potential solving the Poisson equation. The mass density is of course proportional to the gradient of this potential. Therefore, it is possible in principle (if not always in practice) to solve the collisionless Boltzmann equation and Poisson's equation together to obtain the mass density. In the case that the distribution function goes as a power of the energy, the combined equation is called the Lane-Emden equation; the density is proportional to the solution of this equation raised to the power of the polytropic index n. Unfortunately, the coefficient of the proportionality is not a constant, but a generally complicated function. Only in the case of $n = 5$, the Plummer model (Plummer 1911; Binney and Tremaine 2008), does the Lane-Emden equation yield a simple expression for the density.

$$\rho_{\rm P}(r) = \frac{3}{4\pi}\frac{M_{\rm tot} r_0^2}{(r^2+r_0^2)^{5/2}}\,, \tag{1}$$

where r_0 represents "Plummer length". $M_{\rm tot}$ is the total mass of the cluster.

Another well-known model is that of Hernquist, which realizes de Vaucouleurs ' $1/4$ law, the relationship between surface brightness and distance from the center for elliptic galaxies (de Vaucouleurs 1948). Although the Hernquist model is phenomenological, it has been widely applied, and with much success (Hernquist 1990). The density in the Hernquist model is given by:

$$\rho_{\rm H}(r) = \frac{M_{\rm tot}}{2\pi}\frac{r_0}{r}\frac{1}{(r+r_0)^3}\,. \tag{2}$$

Note that the Hernquist model diverges at $r = 0$, whereas in the Plummer model, the density distribution converges gently at the center.

For a globular cluster without an IMBH, we consider the Plummer model and the Hernquist model.

2.2. Mass distribution around an IMBH

If a globular cluster includes an IMBH, the exchange of orbital energies causes the distribution of stars to take a characteristic form. Here we make several assumptions: 1) The distribution of stars is represented by a single-particle distribution function; 2) The mass of the IMBH is much smaller than the mass of the globular cluster core; 3) For simplicity, all the stars around the IMBH have the same mass; 4) The distribution of stars is independent of angular momentum. Under these assumptions, the static solution for the density distribution of stars by the Fokker-Planck equation obeys a specific power law and is known as the Bahcall-Wolf cusp (Bahcall and Wolf 1976; Merritt 2013).

$$\rho_{\rm B}(r) \propto r^{-7/4}\,. \tag{3}$$

The Bahcall-Wolf cusp has been verified by N-body simulation for stellar systems around a massive object (Preto et al. 2004). In contrast to the Plummer models, in a Bahcall-Wolf cusp the mass density diverges at the center. To consider lensing by a Bahcall-Wolf cusp, it is necessary to consider the mass of the IMBH itself.

3. Geodesic equations

3.1. Geodesic equations for the spherically symmetric model

In this paper, we consider the equilibrium state for globular clusters with spherical symmetry. Therefore, spacetime is described by the Schwarzschild metric (Misner et al. 1973; Hartle 2003).

$$\begin{aligned}{\rm d}s^2 = &-\left(1+\frac{2}{c^2}\Psi(r)\right){\rm d}\,(ct)^2+\left(1+\frac{2}{c^2}\Psi(r)\right)^{-1}{\rm d}r^2\\ &+r^2\left({\rm d}\theta^2+\sin^2\theta{\rm d}\phi^2\right)\,,\end{aligned} \tag{4}$$

where $\Psi(r)$ corresponds to the Newtonian gravitational potential.

From the Schwarzschild metric, geodesic equations may be derived. Hereafter we define the time component as

$$w \equiv ct\,. \tag{5}$$

The geodesic equations are as follows:

$$\begin{aligned}\frac{{\rm d}^2 w}{{\rm d}\lambda^2} =& -\frac{2}{c^2}\frac{{\rm d}\Psi}{{\rm d}r}\left(1+\frac{2}{c^2}\Psi\right)\frac{{\rm d}w}{{\rm d}\lambda}\frac{{\rm d}r}{{\rm d}\lambda}\,,\\ \frac{{\rm d}^2 r}{{\rm d}\lambda^2} =& -\frac{2}{c^2}\frac{{\rm d}\Psi}{{\rm d}r}\left(1+\frac{2}{c^2}\Psi\right)\left(\frac{{\rm d}w}{{\rm d}\lambda}\right)^2\\ &+\frac{2}{c^2}\frac{{\rm d}\Psi}{{\rm d}r}\left(1+\frac{2}{c^2}\Psi\right)^{-1}\left(\frac{{\rm d}r}{{\rm d}\lambda}\right)^2\\ &+r\left(1+\frac{2}{c^2}\Psi\right)\left(\frac{{\rm d}\vartheta}{{\rm d}\lambda}\right)^2\end{aligned} \tag{6}$$

$$+ r\sin^2\vartheta\left(1+\frac{2}{c^2}\Psi\right)\left(\frac{\mathrm{d}\phi}{\mathrm{d}\lambda}\right)^2, \tag{7}$$

$$\frac{\mathrm{d}^2\vartheta}{\mathrm{d}\lambda^2} = -\frac{2}{r}\frac{\mathrm{d}r}{\mathrm{d}\lambda}\frac{\mathrm{d}\vartheta}{\mathrm{d}\lambda} + \sin\vartheta\cos\vartheta\left(\frac{\mathrm{d}\phi}{\mathrm{d}\lambda}\right)^2, \tag{8}$$

$$\frac{\mathrm{d}^2\phi}{\mathrm{d}\lambda^2} = -\frac{2}{r}\frac{\mathrm{d}r}{\mathrm{d}\lambda}\frac{\mathrm{d}\phi}{\mathrm{d}\lambda} - \frac{2\cos\vartheta}{\sin\vartheta}\frac{\mathrm{d}\vartheta}{\mathrm{d}\lambda}\frac{\mathrm{d}\phi}{\mathrm{d}\lambda}. \tag{9}$$

Because we consider a null geodesic, we have introduced the parameter λ instead of the world interval s. Moreover, because the trajectory of light can be modeled in a plane, when we notice one trajectory of light, we can ignore the ϕ components. Hereafter we set $\vartheta = \pi/2$.

3.2. Derivation of potential term for models

We consider four models for globular clusters. When there is no IMBH, the densities given by equations (1) and (2) correspond to the potentials

$$\Psi_{\mathrm{P}}(r) = -\frac{GM_{\mathrm{tot}}}{(r^2+r_0^2)^{1/2}}, \tag{10}$$

$$\Psi_{\mathrm{H}}(r) = -\frac{GM_{\mathrm{tot}}}{r+r_0}, \tag{11}$$

where Ψ_{P} and Ψ_{H} refer to the potentials in the Plummer and Hernquist models, respectively. When the globular cluster includes an IMBH, we set a Bahcall-Wolf cusp at the center. Outside the cusp, the effect of the IMBH is tiny. At the boundary of the cusp $r = R$, we connect smoothly with the Plummer or Hernquist model. In connecting the models, we first focus on the continuity of the terms of the geodesic equation. Then we set the first derivative of the potential to be continuous.

For the Plummer model, in the inner region of the model ($r < R$), the potential is then

$$\Psi_{\mathrm{P+B(in)}}(r) = -\frac{GM_{\mathrm{BH}}}{r} - \frac{GM_{\mathrm{tot}}}{(R^2+r_0^2)^{1/2}} + \frac{64}{5}\pi GR^2\rho_0\left[\left(\frac{r}{R}\right)^{1/4} - 1\right], \tag{12}$$

$$\frac{\mathrm{d}\Psi_{\mathrm{P+B(in)}}(r)}{\mathrm{d}r} = \frac{GM_{\mathrm{tot}}}{r^2} + \frac{16}{5}\pi GR\rho_0\left(\frac{r}{R}\right)^{-3/4}. \tag{13}$$

In the outer region of the model ($r > R$), the potential is

$$\Psi_{\mathrm{P+B(out)}}(r) = -\frac{GM_{\mathrm{BH}}}{r} - \frac{GM_{\mathrm{tot}}}{(r^2+r_0^2)^{1/2}}, \tag{14}$$

$$\frac{\mathrm{d}\Psi_{\mathrm{P+B(out)}}(r)}{\mathrm{d}r} = \frac{GM_{\mathrm{tot}}}{r^2} + \frac{GM_{\mathrm{tot}}r}{(r^2+r_0^2)^{3/2}}. \tag{15}$$

To satisfy the condition of connection at the boundary ($r = R$), the density parameter ρ_0 must be

$$\rho_0 = \frac{5M_{\mathrm{tot}}}{16\pi(R^2+r_0^2)^{3/2}}. \tag{16}$$

Similarly, for the Hernquist model, in the inner region($r < R$), the potential is

$$\Psi_{\mathrm{H+B(in)}}(r) = -\frac{GM_{\mathrm{BH}}}{r} - \frac{GM_{\mathrm{tot}}}{R+r_0} + \frac{64}{5}\pi GR^2\rho_0\left[\left(\frac{r}{R}\right)^{1/4} - 1\right], \tag{17}$$

$$\frac{\mathrm{d}\Psi_{\mathrm{H+B(in)}}(r)}{\mathrm{d}r} = \frac{GM_{\mathrm{tot}}}{r^2} + \frac{16}{5}\pi GR\rho_0\left(\frac{r}{R}\right)^{-3/4}. \tag{18}$$

In the outer region of the model ($r > R$), the potential is

$$\Psi_{\mathrm{H+B(out)}}(r) = -\frac{GM_{\mathrm{BH}}}{r} - \frac{GM_{\mathrm{tot}}}{r+r_0}, \tag{19}$$

$$\frac{\mathrm{d}\Psi_{\mathrm{H+B(out)}}(r)}{\mathrm{d}r} = \frac{GM_{\mathrm{tot}}}{r^2} + \frac{GM_{\mathrm{tot}}r}{(r+r_0)^2}. \tag{20}$$

In the Hernquist model, the density parameter ρ_0, which ensures that the boundary conditions match at the point where $r = R$, turns out to be

$$\rho_0 = \frac{5M_{\mathrm{tot}}}{16\pi R(R+r_0)^2}. \tag{21}$$

3.3. Choice of parameters

For consideration of GL by globular clusters, we must fix the values of some parameters. The mass of the IMBH M_{BH}, the radius of the Bahcall-Wolf cusp R, the total mass of the lensing object M_{tot}, and radius of the lensing object r_{lens} should all be considered. Because, in both the Plummer and Hernquist models, a scale length r_0 is included, we must decide on its value as well. For the null geodesic, we must consider the distance between the center of the globular cluster and the background object r_{star}; we must also consider the distance x_{e} from the Earth to the center of the globular cluster.

Both the Plummer model and the Hernquist model include a length parameter r_0 (equations (1) and (2)), a characteristic quantity that determines the shape of the density distribution. In order to compare the two models, we wish to make the mass contained within radius r_0 approximately the same in both. To do this, we use a relation between r_0 and r_{lens}. For the Plummer model, we set $r_0 = r_{\mathrm{lens}}/2$:

$$\begin{aligned} M_{\mathrm{P}}(r_{\mathrm{lens}}) &= \int_0^{r_{\mathrm{lens}}} \rho_{\mathrm{P}}(r)\cdot 4\pi r^2\mathrm{d}r \\ &= \frac{M_{\mathrm{tot}}r_{\mathrm{lens}}^3}{\left(r_{\mathrm{lens}}^2+(r_{\mathrm{lens}}/2)^2\right)^{3/2}} \\ &\simeq 0.72\,M_{\mathrm{tot}}. \end{aligned} \tag{22}$$

For the Hernquist model, we set $r_0 = r_{\mathrm{lens}}/5$:

$$\begin{aligned} M_{\mathrm{H}}(r_{\mathrm{lens}}) &= \int_0^{r_{\mathrm{lens}}} \rho_{\mathrm{H}}(r)\cdot 4\pi r^2\mathrm{d}r \\ &= \frac{M_{\mathrm{tot}}r_{\mathrm{lens}}^2}{(r_{\mathrm{lens}}+r_{\mathrm{lens}}/5)^2} \\ &\simeq 0.69\,M_{\mathrm{tot}}. \end{aligned} \tag{23}$$

For both models, about 70% of the total mass is thus within the radius of the lensing object.

In this paper, the mass of the IMBH is fixed at $M_{\mathrm{BH}} = 10^4\,M_\odot$. The upper bound of the distance to the background star is fixed at $r_{\mathrm{star}} < 10^6$ lyr. The globular cluster is assumed to belong to the Milky Way; catalogs of Milky Way globular clusters have been published (Harris 1996; Hilker et al. 2020). The parameters (total mass, calculated radius from apparent dimension, and distance from the Earth) of the clusters in the present paper are chosen to be typical of relatively large Milky Way globular clusters according to the catalogs:

- $1 \times 10^6 \leq M_{\rm tot} \leq 5 \times 10^6\, M_\odot$
- $10 \leq r_{\rm lens} \leq 100\,{\rm lyr}$
- $1 \times 10^4 \leq x_{\rm e} \leq 10 \times 10^4\,{\rm lyr}$

Here $x_{\rm e}$ means the distance from the Earth to the center of the globular cluster. The boundary of Bahcall-Wolf cusp is fixed at $R = 1\,{\rm lyr}$.

4. Effect of gravitational lensing

4.1. Model settings

Various physical and geometrical quantities required for analyzing the GL effect of globular clusters will now be defined. Figure 1 shows the positional relationship between the Earth, globular cluster, and background star. Even if spacetime is curved by gravity, the trajectory of light can be analyzed in a plane. The center of the globular cluster is defined as the origin. Then the Earth is set at $(x_{\rm e}, 0)$. This position is denoted as point E. A background star is positioned at point S. Because of the effect of GL, however, this star appears to observers on Earth to be at point S'. The angle between the x-axis and line segment $\overline{ES'}$ is defined as θ. Then the deflection angle (angle between line segments $\overline{ES}$ and $\overline{ES'}$) is defined as Θ. The intersection point of the y-axis and line segment $\overline{ES'}$ is defined as the "impact parameter" $y_{\rm lens}$. The relationship between the impact parameter and θ is

$$\tan\theta = \frac{y_{\rm lens}}{x_{\rm e}}\,. \tag{24}$$

The distance between the center of the globular cluster and the background star is given by $r_{\rm star}$.

4.2. Typical example – ω Centauri

As an example for our study, one well-known globular cluster is selected and verified. ω Centauri is the most massive globular cluster of the Milky Way. The existence of an IMBH in ω Centauri has been discussed from both theoretical and observational perspectives (Noyola et al. 2010; Haggard et al. 2013; Baumgardt et al. 2019). The effect of the GL will be calculated using the known parameters of ω Centauri: $M_{\rm tot} = 4 \times 10^6\, M_\odot$, $r_{\rm lens} = 82\,{\rm lyr}$, $x_{\rm e} = 1.56 \times 10^4\,{\rm lyr}$. For this calculation, $r_{\rm star}$ is fixed at $5 \times 10^5\,{\rm lyr}$ (van de Ven et al. 2006; D'Souza and Rix 2013).

When the cluster excludes the IMBH, the mass distribution is given by the Plummer model or the Hernquist model. The deflection angle is shown in figure 2. For the case of the Hernquist model (hereafter, model H), the deflection angle increases sharply as the impact parameter decreases. Conversely, for the case of the Plummer model (hereafter, model P), the deflection angle approaches a constant value at $y_{\rm lens} = 0$. This is due to the difference in gravitational potential between models: for model P, the potential flattens at the center, but for model H, the potential sharpens there.

When the cluster includes an IMBH, the deflection angle dramatically changes at small impact parameters. For the case of the Plummer model with an IMBH (hereafter, model P-BH), the difference of angle becomes significant at $y_{\rm lens} \leq 20\,{\rm lyr}$ (figure 3). Although the boundary of Bahcall-Wolf cusp is fixed at 1 lyr, the trajectory of light is affected well outside this radius. Due to the effect of the IMBH, the angle diverges at $r \simeq 0$. For the case of the Hernquist model with an IMBH (hereafter, model H-BH), although the effect of the IMBH (or cusp) appears at small impact parameters, it is not as clear as in the case of model P-BH (figure 4). Perhaps this result is caused by H-BH's less extreme potential slope near the center.

4.3. Dependence on parameters

We investigate the effect of changing the parameters on the deflection angle. The standard values of the parameters are as follows:

- Total mass of lensing object: $M_{\rm tot} = 10^6\, M_\odot$
- Radius of lensing object: $r_{\rm lens} = 50\,{\rm lyr}$
- Distance from the Earth: $x_{\rm e} = 5 \times 10^4\,{\rm lyr}$
- Distance between the center of the globular cluster and the background object: $r_{\rm star} = 5 \times 10^5\,{\rm lyr}$

The above four parameters are then changed one by one, with the following results:

Figure 5 shows the dependence of the deflection angle on total mass $M_{\rm tot}$. As $M_{\rm tot}$ increases, the angle increases because gravity strengthens. Figure 6 shows the dependence of the deflection angle on the radius of the lensing object $r_{\rm lens}$. The lensing effect increases as the mass is concentrated in a narrower area.

We also show the dependence on the distance between the globular cluster and the Earth. The angle θ changes as the distance between the Earth and the globular cluster changes. Figure 7 shows the θ dependence of the deflection angle. Since we are considering globular clusters belonging to the Milky Way, the upper limit of the distance is set to $10^5\,{\rm lyr}$. The distance dependence of the angle, therefore, seems from the figure to be insignificant.

Finally, we consider the dependence on the distance to the background object (figure 8). As the distance to the background object increases, the angle approaches a limiting curve that, except in model P, rises steeply at low impact parameters.

4.4. Observability of gravitational lensing effects

Finding the trajectories of two light beams reaching the Earth from the same astronomical object generally requires solving a boundary value problem. The trajectory that connects the Earth and astronomical object is determined. As a simple case, we consider a situation where the Earth, lensing object, and background object are aligned (figure 9). In this situation, the separation angle of the two trajectories due to GL can be calculated easily: it becomes 2Θ, or twice the refraction angle. If the separation angle is large enough, multiple celestial images will be observed. Even if the separation angle is small, the effect of GL will increase the brightness of the background object.

The Earth, lensing object, and background object are aligned when the initial emission angle and the refraction angle are equal. Therefore, for each model, the situation where the initial emission angle and the refraction angle coincide has been investigated. For analysis, we consider the parameters given by the case of ω Centauri. The results are shown in table 1.

From table 1, the presence of a black hole affects the separation angle by about 10×10^{-2} arcsec.

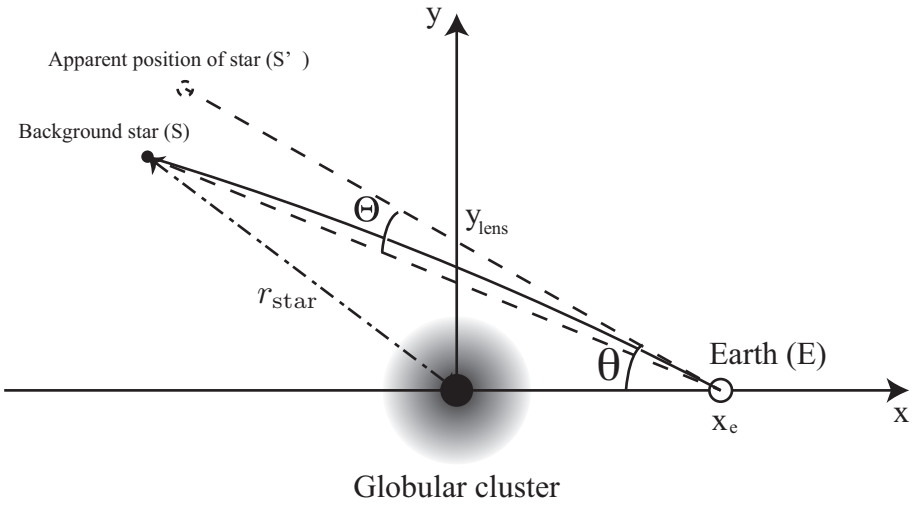

Fig. 1. Schematic of the positional relationship between the Earth, globular cluster, and background star. The center of the globular cluster is defined as the origin, and the trajectory of light from the background star to the Earth (solid line) is analyzed.

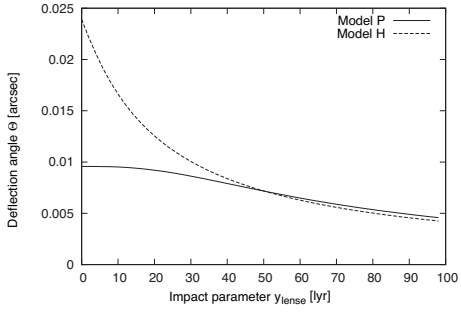

Fig. 2. The deflection angle by the Plummer model (Model P) and the Hernquist model (Model H) as a function of impact parameter.

Table 1. Impact factor $y_{\rm lens}$ when initial emission angle equals refraction angle Θ

Models	$y_{\rm lens}\,[\times 10^3\,{\rm lyr}]$	$\Theta\,[\times 10^{-2}\,{\rm arcsec}]$
Model P	0.724	0.957
Model P-BH	10.1	13.1
Model H	1.81	2.39
Model H-BH	10.8	14.2

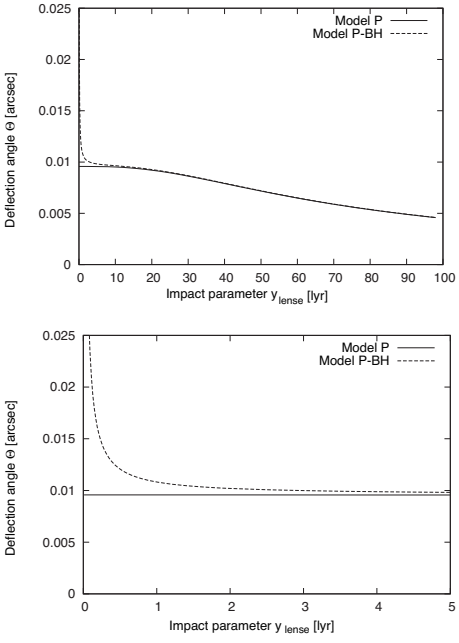

Fig. 3. Comparison of deflection angle with and without IMBH in the Plummer model. The figure on the right is an enlarged view of $y_{\rm lens}$ from the figure on the left.

We have investigated the effects of other parameters also. The value that maximizes the separation angle is selected within the range of the parameters treated in section 4.3:

- $M_{\rm tot} = 5 \times 10^6\,M_\odot$,
- $r_{\rm lens} = 10\,{\rm lyr}$,
- $x_{\rm e} = 1 \times 10^4\,{\rm lyr}$,
- $r_{\rm star} = 10 \times 10^5\,{\rm lyr}$.

With this choice of parameters, the separation angle of the H-BH model takes its maximum value, about $0.''76$. The smallness of this angle makes it difficult to observe the lensing phenomenon from the ground due to complications with the Earth's atmosphere.

4.5. Case of dark globular cluster

As we mentioned in section 3, globular clusters in the Milky Way have been cataloged (Harris 1996; Hilker et al. 2020). Our calculations indicate that the GL effect is small even in the case of ω Centauri. It is unlikely that a new globular cluster will be found near the Earth. It takes enough time for known globular clusters to be close to Earth. Here we consider a different situation.

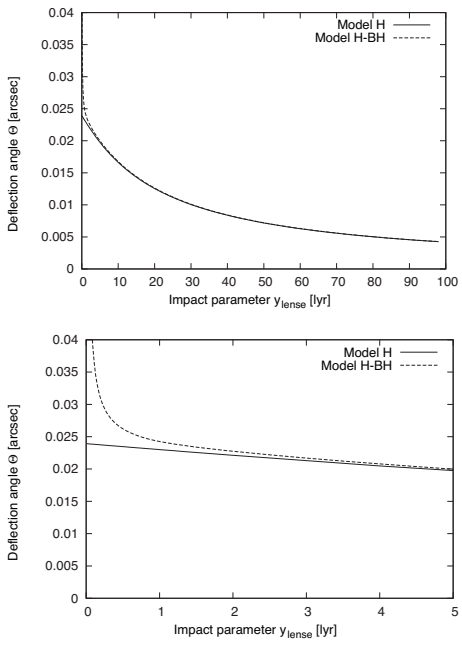

Fig. 4. Comparison of deflection angle with and without IMBH in the Hernquist model. The figure on the right is an enlarged view of $y_{\rm lens}$ from the figure on the left.

Suppose that cold dark matter can condense into something like a globular cluster (Carr and Lacey 1987). Such an object would not emit light by itself and would not be included in the existing catalogs of globular clusters. If such a "dark globular cluster" exists and is closer to the Earth than other globular clusters, how much of a GL effect would it produce?

Here we consider dark globular clusters that can be treated by the Hernquist model, with and without IMBHs. We fix two parameters:

- $x_{\rm e} = 5 \times 10^3\,{\rm lyr}$
- $r_{\rm star} = 5 \times 10^5\,{\rm lyr}$

Figure 10 shows the deflection angle when the radius of the lensing object is changed. In this figure, the total mass of the globular cluster is fixed at $M_{\rm tot} = 10^6\,M_\odot$. Figure 11 shows the deflection angle when the total mass of the lensing object is changed. In this figure, the radius of the globular cluster is fixed at $r_{\rm lens} = 50\,{\rm lyr}$.

In these models, the deflection angle can be up to about $2''$. If a dark globular cluster containing an IMBH is within a few thousand light years from the Earth, it may be detected by the GL effect in future observations.

5. Conclusion

We considered a method to determine the presence of an IMBH in a globular cluster by examining the GL effect. Under the assumption of spherical symmetry, we considered the mass distribution of globular clusters with and without IMBHs, and then calculated the separation angle of light trajectories based on this. (Note that, in this study, it was assumed that the trajectories could pass through the interior of the globular cluster, but such a pass-through might be impossible if the globular cluster is extremely dense. In that case, background objects could not be seen.)

A catalog of globular clusters in the Milky Way Galaxy has been published (Harris 1996; Hilker et al. 2020). Typical parameters, based on those listed in this catalog, served as input to see how strong a GL effect a cluster can produce. For ω Centauri, a dense globular cluster that is the most massive belonging to the Milky Way, the separation angle of the GL effect caused by the globular cluster with an IMBH was found to be on the order of sub-milliarcseconds. For other globular clusters belonging to the Milky Way, the separation angle would be even smaller.

Observing multiple images may be difficult due to the small separation angle of the GL. The brightening effect caused by GL may be more easily observed. Light that travels through multiple trajectories from background objects can be concentrated onto the Earth by the GL effect, which causes sources to appear brighter than they are in reality. Systematic observations of the GL effect on galaxies have been made in the past (Tyson et al. 1990; Dahle et al. 2002; Kubo et al. 2009; Jaelani et al. 2020). We are considering similar surveys for globular clusters.

This method has been applied to MACHO observations with small separation angles (Alcock et al. 2000). If a single observation reveals that the brightening effect of the globular cluster due to the GL effect is quite strong, the density distribution of the globular cluster may be high, suggesting the presence of an IMBH. By observing the change in the brightening rate of a globular cluster as it passes between background objects and the Earth, it may be possible to detect the presence or absence of an IMBH, but such continuous observations would require a more extensive observation program than the MACHO Project. Quantitative evaluation of brightening due to the GL effect will be derived in future work.

The authors would like to thank Shigeyuki Karino, Takahiko Matsubara, Kouji Nakamura, Hiroyuki Nakano, Hisaaki Shinkai, and Kousuke Sumiyoshi for their useful discussion at 32nd RIRONKON symposium (Dec. 25-27, 2019, National Astronomical Observatory, Japan). We would like to thank Editage (www.editage.com) for English language editing.

References

Alcock, C., et al. 2000, ApJ, 542, 281
Bahcall, J. N., & Wolf, R. A. 1976, ApJ, 209, 214
Baumgardt, H., et al. 2019, MNRAS, 488, 5340
Baumgardt, H., Hut, P., Makino, J., McMillan, S., & Portegies Zwart, S. 2003, ApJ, 582, L21
Binney, J., & Tremaine, S. 2008, Galactic Dynamics, 2nd ed. (Princeton, NJ: Princeton University Press)
Bukhmastova, Yu. L. 2003, Astron. Lett., 29, 214
Carr, B. J., & Lacey, C. G. 1987, ApJ, 316, 23
Dahle, H., Kaiser, N., Irgens, R. J., Lilje, P. B., & Maddox, S. J. 2002, ApJS, 139, 313
den Brok, M., van de Ven, G., van den Bosch, R., & Watkins, L. 2014, MNRAS, 438, 487
de Vaucouleurs, G. 1948, Annales d'Astrophysique, 11, 247
D'Souza, R., & Rix, H.-W. 2013, MNRAS, 429, 1887
Event Horizon Telescope Collaboration, et al. 2019, ApJ, 875, L1

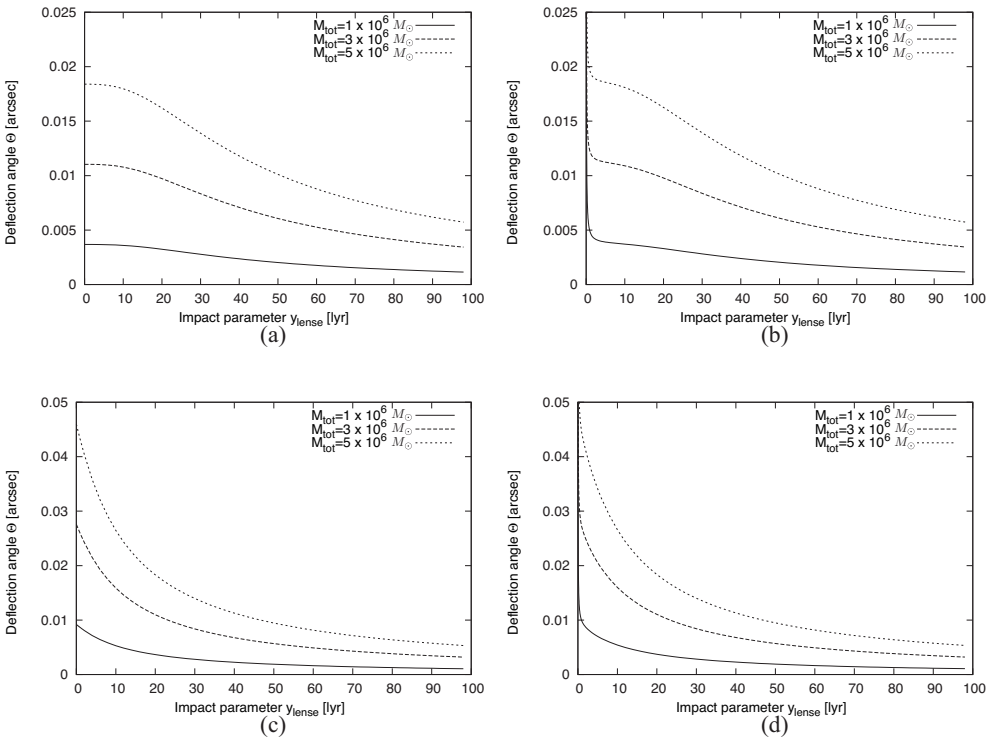

Fig. 5. Dependence of the deflection angle on the total mass M_{tot} for (a) Plummer model, (b) Plummer model with IMBH, (c) Hernquist model, and (d) Hernquist model with IMBH.

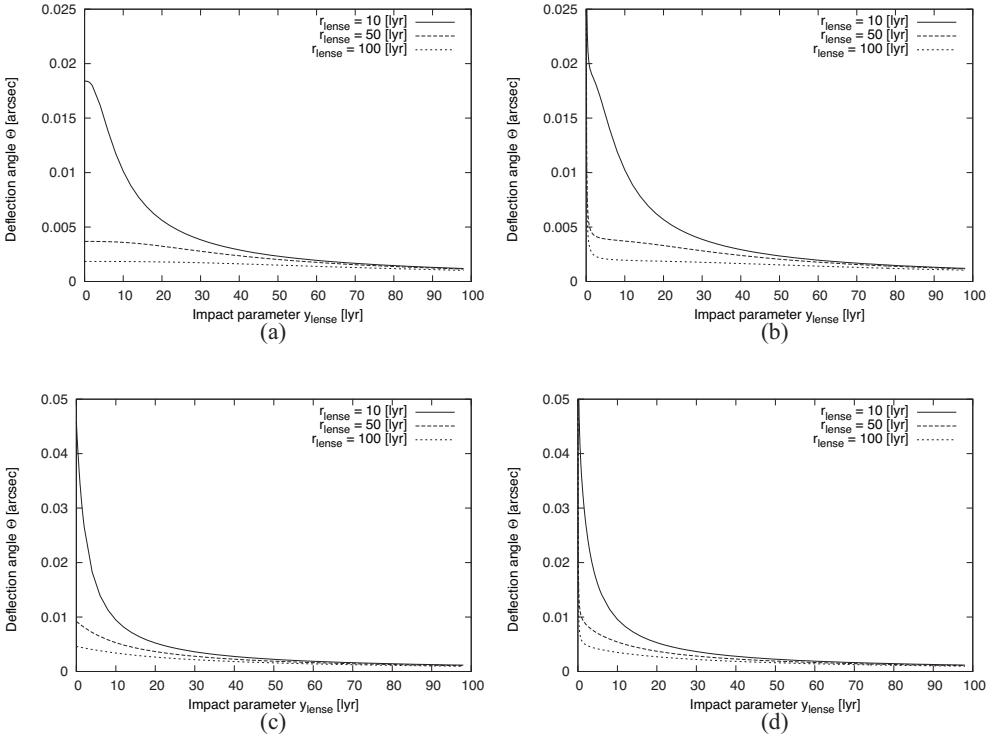

Fig. 6. Dependence of the deflection angle on the radius of the lensing object $r_{\rm lens}$ for (a) Plummer model, (b) Plummer model with IMBH, (c) Hernquist model, and (d) Hernquist model with IMBH.

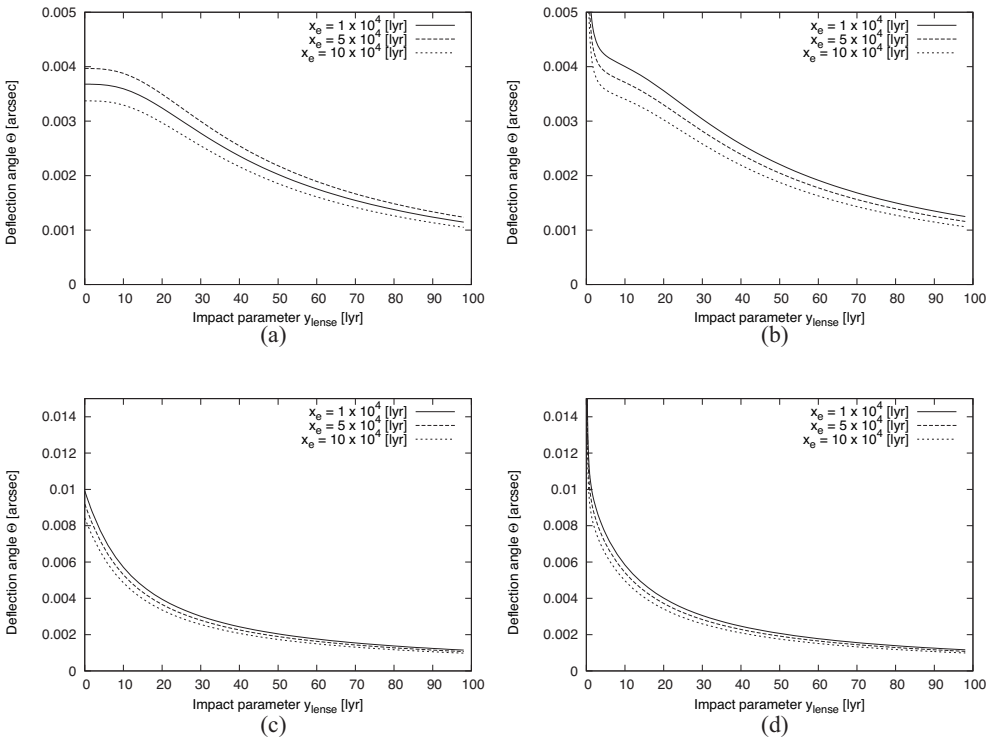

Fig. 7. Dependence of the deflection angle on the distance between a globular cluster and the Earth $x_{\rm e}$ for (a) Plummer model, (b) Plummer model with IMBH, (c) Hernquist model, and (d) Hernquist model with IMBH.

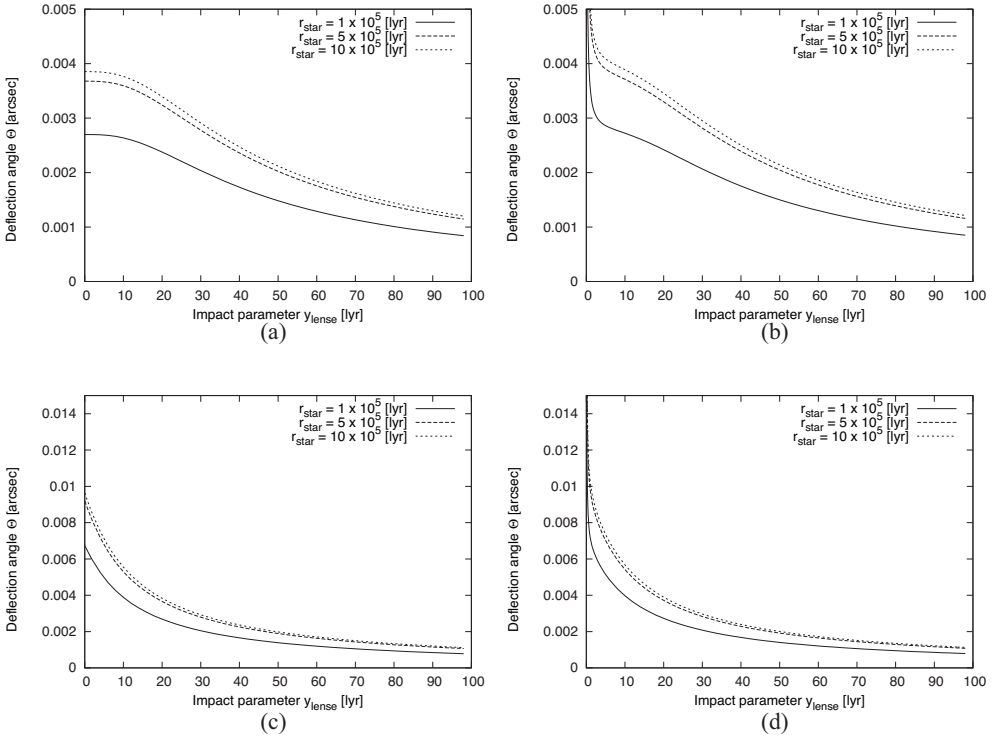

Fig. 8. Dependence of the deflection angle on the distance to a background object r_{star} for (a) Plummer model, (b) Plummer model with IMBH, (c) Hernquist model, and (d) Hernquist model with IMBH.

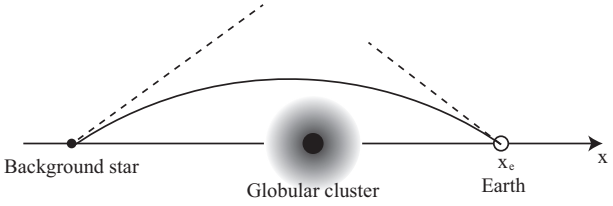

Fig. 9. Schematic of the ideal case in which the Earth, globular cluster, and background star are aligned. Dashed tangential lines indicate the trajectory at the Earth and a background star, respectively. The separation angle becomes twice the refraction angle.

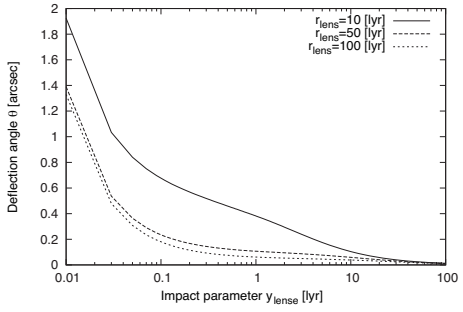

Fig. 10. Comparison of deflection angle when the radius of the lensing object is changed.

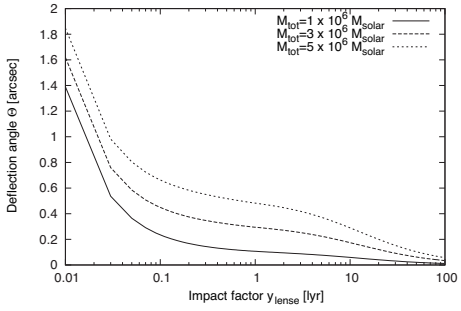

Fig. 11. Comparison of deflection angle when the total mass of the globular cluster is changed.

Ferrarese, L., & Merritt, D. 2000, ApJ, 539, L9
Gebhardt, K., et al. 2000, ApJ, 539, L13
Gerssen, J., van der Marel, R. P., Gebhardt, K., Guhathakurta, P., Peterson, R. C., & Pryor, C. 2002, AJ, 124, 3270
Ghez, A. M., Morris, M., Becklin, E. E., Tanner, A., & Kremenek, T. 2000, Nature, 407, 349
Gillessen, S., Eisenhauer, F., Trippe, S., Alexander, T., Genzel, R., Martins, F., & Ott, T. 2009, ApJ, 692, 1075
Greene, J. E., Strader, J., & Ho, L. C. 2020, ARA&A, 58, 257
Gültekin, K., et al. 2009, ApJ, 698, 198
Haggard, D., Cool, A. M., Heinke, C. O., van der Marel, R., Cohn, H. N., Lugger, P. M., & Anderson, J. 2013, ApJ, 773, L31
Harris, W. E. 1996, AJ, 112, 1487
Hartle, J. B. 2003, Gravity: an introduction to Einstein's general relativity (San Francisco: Addison-Wesley)
Hernquist, L. 1990, ApJ, 356, 359
Hilker, M., Baumgardt, H., Sollima, A., & Bellini, A. 2020, in IAU Symp. 351, Star Clusters: From the Milky Way to the Early Universe, ed. A. Bragaglia et al. (Cambridge, UK: Cambridge University Press), 451
Jaelani, A. T., et al. 2020, MNRAS, 495, 1291
Kains, N., Bramich, D. M., Sahu, K. C., & Calamida, A. 2016, MNRAS, 460, 2025
Kains, N., Calamida, A., Sahu, K. C., Anderson, J., Casertano, S., & Bramich, D. M. 2018, ApJ, 867, 37
Kiselev, A. A., Gnedin, Y. N., Shakht, N. A., Grosheva, E. A., Piotrovich, M. Yu., & Natsvlishvili, T. M. 2008, Astron. Lett., 34, 529
Kubo, J. M., et al. 2009, ApJ, 702, L110
McNamara, B. J., Harrison, T. E., & Anderson, J. 2003, ApJ, 595, 187
Merritt, D. 2013, Dynamics and Evolution of Galactic Nuclei (Princeton, NJ: Princeton University Press)
Misner, C. W., Thorne, K. S., & Wheeler, J. A. 1973, Gravitation (San Francisco: W.H. Freeman & Co.)
Murphy, B. W., Cohn, H. N., & Lugger, P. M. 2011, ApJ, 732, 67
Noyola, E., Gebhardt, K., Kissler-Patig, M., Lützgendorf, N., Jalali, B., de Zeeuw, P. T., & Baumgardt, H. 2010, ApJ, 719, L60
Plummer, H. C. 1911, MNRAS, 71, 460
Preto, M., Merritt, D., & Spurzem, R. 2004, ApJ, 613, L109
Rees, M. J. 1984, ARA&A, 22, 471
Silk, J., & Rees, M. J. 1998, A&A, 331, L1
Tyson, J. A., Valdes, F., & Wenk, R. A. 1990, ApJ, 349, L1
van de Ven, G., van den Bosch, R. C. E., Verolme, E. K., & de Zeeuw, P. T. 2006, A&A, 445, 513